CrossMark

Fabrication of Hydrogels with a Stiffness Gradient Using Limited Mixing in the Hele-Shaw Geometry

D. Lee [1,2] · K. Golden [3] · Md.M. Rahman [1,4] · A. Moran [5,6] · B. Gonzalez [7,8] · S. Ryu [1,9]

Abstract

Hydrogel substrates with a stiffness gradient have been used as a surrogate of the extracellular matrix (ECM) to investigate how cells respond to the stiffness of their surrounding matrix. Various fabrication methods have been proposed to create a stiffness gradient in the hydrogel substrate, and some of them rely on generating a concentration gradient in a prepolymer solution before photo-polymerization. One easy way to do so is to coalesce two prepolymer solution drops of different stiffness values in a narrow confinement formed by two glass surfaces and then to induce polymerization using ultraviolet (UV) light irradiation, as proposed by Lo et al. [Biophys. J. 2000, 79:144–152]. We have improved their method to enable modulating the obtained stiffness gradient and characterized fabricated polyacrylamide (PAAM) gels. We controlled the coalescence and mixing duration of two prepolymer drops using the lab-built Hele-Shaw cell device and glass surfaces with a superhydrophobic barrier. Limited mixing between the drops created a concentration gradient of the gel ingredient, which was converted to a stiffness gradient by UV-based photo-polymerization. Atomic force microscopy (AFM) indentation showed that the fabricated gels had the stiffness gradient zone at the center and that the width of the zone increased with the mixing duration.

Keywords Polyacrylamide hydrogel · Young's modulus · AFM indentation · Drop coalescence · Diffusion

Introduction

The stiffness of the extracellular matrix (ECM) significantly influences various cellular functions through mechanobiological interactions between cells and the ECM [1–4]. For *in vitro* investigations of such effects, hydrogel substrates of uniform elasticity or stiffness, which is quantified by Young's modulus (E), have been used as a surrogate for the ECM [4–6]. Among various hydrogels available for this purpose, polyacrylamide (PAAM) gel has been widely employed because it is transparent and chemically inert, and more importantly, it is easy to modulate the stiffness by adjusting the concentration of acrylamide (monomer) and bis-acrylamide (cross-linker) [7–10].

Because the extracellular environment is physiologically and mechanically inhomogeneous, hydrogel substrates of stiffness variation or gradient can better mimic the ECM of natural or pathological conditions. Accordingly, several techniques were developed to generate a stiffness variation or gradient on a single hydrogel substrate [11]. These techniques can be roughly categorized into several groups depending on their working principle.

The first group generates a concentration gradient of polymer composition in a pre-polymer solution, which becomes a

✉ S. Ryu
    sryu2@unl.edu

1   Department of Mechanical & Materials Engineering, University of Nebraska-Lincoln, Lincoln, NE 68588, USA

2   Present address: Department of Genetics, Cell Biology and Anatomy, University of Nebraska Medical Center, Omaha, NE 68198, USA

3   School of Biological Sciences, University of Nebraska-Lincoln, Lincoln, NE 68588, USA

4   Present address: Department of Mechanical Engineering, University of Louisville, Louisville, KY 40292, USA

5   Department of Agricultural and Biological Engineering, University of Florida, Gainesville, FL 32611, USA

6   Present address: Department of Biomedical Engineering, University of Florida, Gainesville, FL 32611, USA

7   Department of Biomedical Engineering, Georgia Institute of Technology, Atlanta, GA 30332, USA

8   Present address: Department of Biomedical Engineering, Florida International University, Miami, FL 33174, USA

9   Nebraska Center for Materials and Nanoscience, University of Nebraska-Lincoln, Lincoln, NE 68588, USA

SEM

gradient of stiffness after polymerization. The most well-known method in this group is the microfluidics-based method which generates a continuous concentration in a microfluidic channel device [12–17]. Others in the group rely on diffusion-based limited mixing in a confined space [18–20], non-microfluidic gradient makers [21, 22], and convection-alternating flow [23].

The second group controls the degree of polymerization or cross-linking by modulating irradiation for photo-polymerization over a hydrogel. Each method in this group either uses a photo mask to create a gradient of irradiation [21, 24–29], a moving opaque mask to result in a gradient of exposure time [27, 30–35], or a focused beam for micro-projection to localize irradiation [29, 36–39]. Likewise, a similar method was proposed to create stiffness gradient in poly-dimethylsiloxane (PDMS) substrates by exposing curing PDMS to temperature gradient [40].

The third group generates discrete stiffness distribution on hydrogels using micropatterning [41, 42] and microfluidics-based lithography [43]. Finally, the fourth group controls the thickness of hydrogel substrates to create variation in apparent Young's modulus [44–46]. Additionally, stiffness gradient can be generated by gradually freezing and thawing hydrogels [47] or by dipping a hydrogel in its crosslinking solution in a controlled manner [48].

In the presented study, we propose a quick and cost-effective method to fabricate PAAM gel substrates using drop coalescence and limited mixing in the Hele-Shaw cell. Our method is based on the method of Lo et al. to fabricate PAAM gel substrates with a stiffness gradient [18]. They squeezed two drops of the pre-polymer solution of different ratios of acrylamide and bis-acrylamide [fixed acrylamide concentration (8%) and two different bis-acrylamide concentrations (0.048 and 0.48%)] between two glass surfaces. Then, the drops were allowed to coalesce and cross-linked using ultraviolet (UV) light exposure. Although the two drops coalesced, they could not fully mix because of the Hele-Shaw cell formed by the two glass surfaces. As a result, a concentration gradient of bis-acrylamide formed at the interface between the drops, and accordingly a stiffness gradient was generated after photo-polymerization. We have improved the method of Lo et al. for better controlled generation of stiffness gradient and rigorously characterized fabricated PAAM gel substrates.

Our gel fabrication steps are illustrated in Fig. 1. A dumbbell-shaped hydrophilic region was formed on a cover glass, outlined by a superhydrophobic barrier. Then, two PAAM prepolymer drops were placed in the circular wells of the hydrophilic region, one for a lower stiffness and the other for a higher stiffness (Table 1). The drops were squeezed by an amino-silanated glass slide which was lowered by a motorized stage. Thus, two glass surfaces formed a Hele-Shaw cell in which the two drops coalesced upon contact. After a given duration for mixing between the drops, UV light

was shed upon the coalesced drop, creating a PAAM gel from the solution. Obtained stiffness gradient was measured using atomic force microscopy (AFM) indentation. Employing this method, we generated a stiffness gradient zone at the center of the gel (7.9, 5.6 and 4.1 kPa/mm for 9, 36, and 81-min long mixing duration, respectively) and two static stiffness zones at the ends of the gel (soft side: 2.0–2.3 kPa, stiff side: 34.0–35.3 kPa). The proposed gel fabrication method provides an easy and cost effective method for making a stiffness gradient on a PAAM gel, which can be easily adopted in various research settings.

Materials and Methods

Hele-Shaw Cell Device

The proposed method for producing a stiffness-gradient hydrogel requires fine control when squeezing the drops. For this purpose, we built the motorized Hele-Shaw cell device as shown in Fig. 2(a). It mainly consisted of the motorized stage which was assembled using Makeblock parts (Makeblock Co., China), a DC power source, a vacuum pump (modified Whisper 100 Aquarium Air Pump; Tetra, Blacksburg, VA), the Hele-Shaw cell composed of two glass surfaces, an acrylic base plate for holding the bottom glass surface of the Hele-Shaw cell, and an LED lamp (Adafruit Industries, New York City, NY) for bottom-up illumination. Energized by the DC power source, the DC motor (30 rpm at 6 V) of this motorized stage rotated the threaded rod, which drove the vertical movement of two forks that housed suction cups. Connected to the vacuum pump, the suction cups held the top glass surface of the Hele-Shaw cell using negative pressure. The rotational speed of the motor could be lowered by decreasing the voltage from the power source from 6 V to 0.8 V. Thus, it was possible to decrease the lowering speed of the top surface of the Hele-Shaw cell to 44.5 ± 2.6 μm/s (mean ± standard deviation; $N = 6$ measurements).

Glass Surface Preparation

As shown in Fig. 2(b), the Hele-Shaw cell of our setup was formed by two glass surfaces. In order to fix fabricated PAAM gel on the top glass surface, we prepared amino-silanated slide glass pieces via the following procedures [50–52]. Slide glass pieces (75 mm × 25 mm × 1.2 mm) were shaken at 55 rpm in 0.2 M HCl overnight at room temperature and rinsed with deionized water (diH$_2$O). In the same way, the coverslips were treated using 0.1 M NaOH for an hour and rinsed with diH$_2$O. The same surface treatment procedure for the coverslips was repeated with 1% (v/v) 3-aminopropyltrimethoxysilane (Sigma-Aldrich, St. Louis, MO) in diH$_2$O and 0.5%
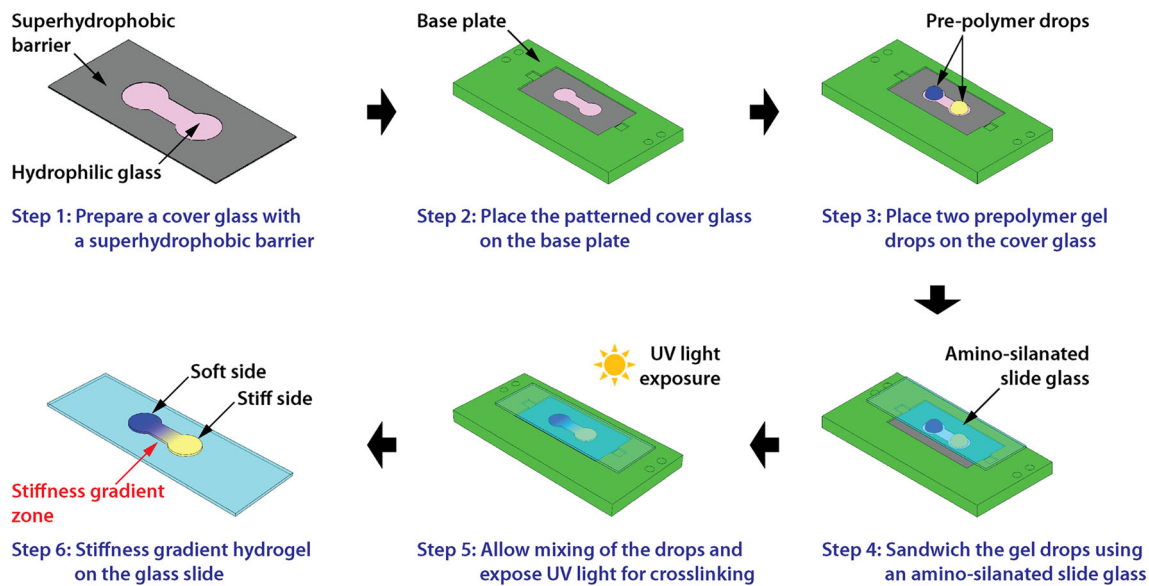
Fig. 1 Fabrication procedure of a hydrogel substrate with a stiffness gradient using limited mixing in the Hele-Shaw cell

glutaraldehyde (Sigma-Aldrich, St. Louis, MO) in phosphate buffered saline (PBS; Amresco, Solon, OH) subsequently.

The bottom glass surface contained a superhydrophobic pattern to control the motion and flow of liquid drops. For this purpose, we made the superhydrophobic barrier pattern on a cover glass (24 mm × 50 mm × 0.13–0.16 mm) as briefly follows (Fig. 2(c)). First, a dumbbell-shaped "sticker" was made out of vinyl film (Grafix Cling Film; Grafix Plastics, OH) using AutoCAD (Autodesk, San Rafael, CA) and a cutting plotter (Silhouette CAMEO; Silhouette America, UT). Next, the sticker was attached to a clean cover glass. Then, hydrophobic spray (WX2100; Cytonix Corp., Beltsville, MD; contact angle of water: 154° [53]) was applied to the coverslip, masked with the said sticker, and allowed to dry for two days [54]. Finally, the sticker was detached from the coverslip, forming the superhydrophobic barrier surrounding the exposed hydrophilic glass pattern.

Flow Visualization of Drop Coalescence and Mixing

In order to test the developed Hele-Shaw cell device, we visualized liquid drop coalescence and following mixing using dyed water drops. A clean slide glass and a cover glass with the superhydrophobic barrier were used to form the Hele-Shaw cell, and two water drops of 50 μL in volume were placed each in the circular well part of the hydrophilic glass pattern of the cover glass. For visualization, the water drops

Table 1 Polyacrylamide (PAAM) gel compositions

PAAM gel	Acrylamide % (w/v)	Bis-acrylamide % (w/v)	Nominal Young's modulus (kPa) [49]
Soft side	8	0.048	2.6 ± 0.8
Stiff side	8	0.48	40.4 ± 2.4

were colored in blue and yellow using food dyes (McCormick & Company, Baltimore, MD), respectively. Then the drops were squeezed in the Hele-Shaw cell, and their coalescence and following mixing were recorded with two digital cameras (Canon EOS Rebel T3; Canon, Tokyo, Japan for top view imaging, and Pentax K-01; Ricoh, Tokyo, Japan for front view imaging).

Janus Gel Fabrication

Acrylamide and bis-acrylamide (Bio-Rad, Hercules, CA) of desired concentrations were mixed with PBS to prepare two pre-polymer solutions for the soft and stiff PAAM gels (Table 1). For photo-polymerization, 0.5% (w/v) of Irgacure 2959 (Ciba Specialty Chemicals, Basel, Switzerland) was added to the pre-polymer solutions, and the solutions were degassed for 15 min [26, 49]. The containers of the solutions were wrapped with aluminum foil to prevent possible photo-polymerization by ambient light.

We fabricated PAAM gels with a stiffness gradient through the following steps (Fig. 1). The superhydrophobic patterned cover glass was adhered to the base plate of the Hele-Shaw cell device (Fig. 2(b)) using 20 water droplets (about 5 μL each) positioned along the perimeter of the cover glass. Next, two drops of the prepared pre-polymer solutions were placed on the hydrophilic region of the cover glass, i.e., bare glass part; one drop for soft gel on one circular well, and one drop for stiff gel the opposite well (Table 1). Then the amino-silanated slide glass was attached to the suction cups and checked to maintain a level position. When level, the slide glass was lowered onto the PAAM gel drops using the motorized stage. This process squeezed the drops between the two glass surfaces, eventually causing them to coalesce. Next, the solution was allowed to mix
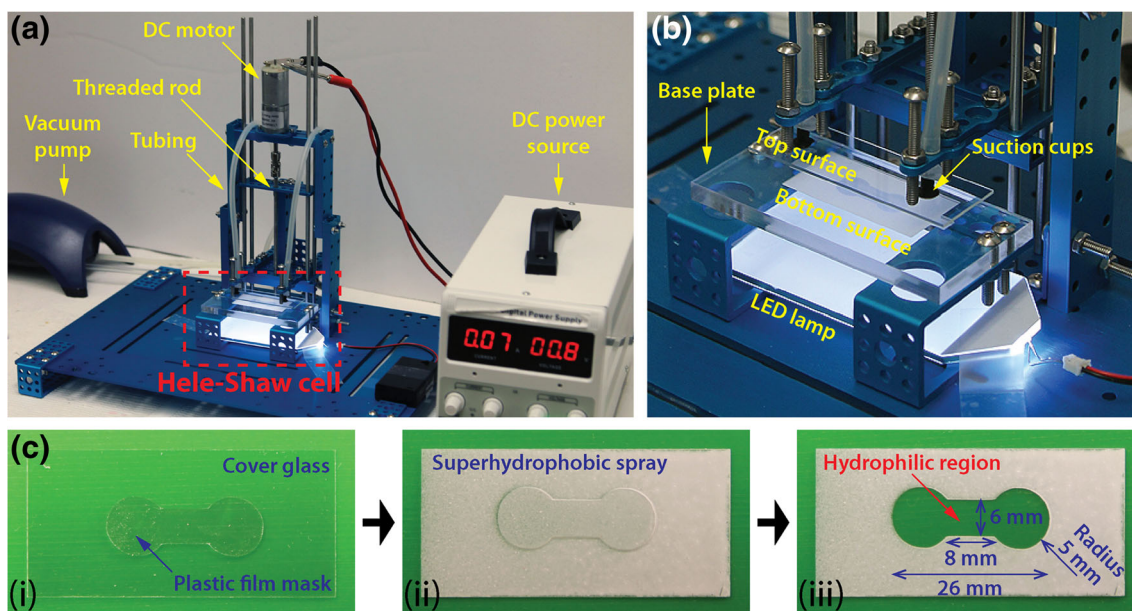
Fig. 2 Hele-Shaw cell device used for fabrication of PAAM gels with stiffness gradient. (A) Whole view of the device consisting of the motorized stage, the Hele-Shaw cell, the vacuum pump, and the DC power source. (B) Magnified view of the Hele-Shaw cell consisting of the top and bottom glass surfaces, the bottom plate to hold the bottom glass surface, two suction cups to hold the top glass surface, and the LED lamp for illumination. (C) Steps to create a hydrophobic barrier pattern on a hydrophilic cover glass. (i) A dumbbell-shaped plastic film mask was placed on a cover glass. (ii) Superhydrophobic spray was applied to the masked cover glass. (iii) Removal of the mask created a hydrophilic glass area surrounded by superhydrophobic coating
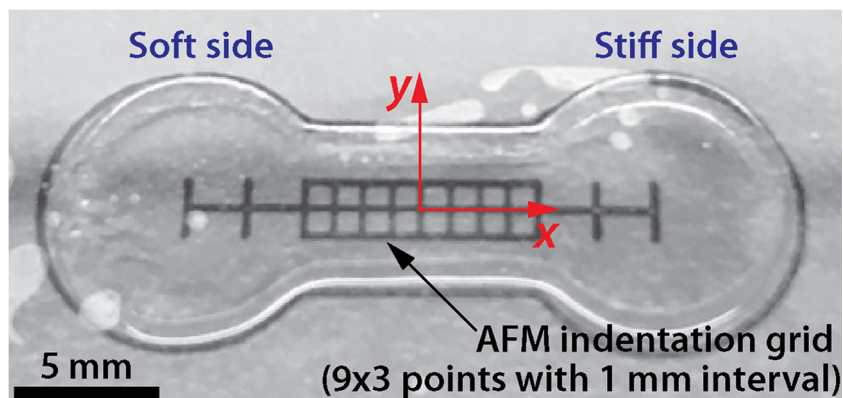
for a given period of time (9, 36 and 81 min) and then exposed to UV light for 30 min for photo-polymerization using a high intensity UV lamp (not pictured in Fig. 2(a); B-100AP; UVP, Upland, CA). Finally, the PAAM gel, which still sat between the two glass surfaces, was submerged into PBS for two hours for easier separation from the bottom glass surface. The fabricated PAAM gel was washed twice in fresh PBS for five minutes. Figure 3 shows a fabricated PAAM gel.

Young's Modulus Measurement

In order to measure the Young's modulus (E) distribution of the fabricated PAAM gels, the AFM indentation method was conducted using MFP-3D-BIO AFM (Asylum Research, Santa Barbara, CA) and V-shaped colloidal probes (Novascan

Technologies, Ames, IA; nominal diameter of the borosilicate glass tip = 12 μm, nominal spring constant = 0.06 N/m). The detailed AFM indentation method is shown in our previous study [52], and a brief overview is given here. A 9×3 rectangular grid with a grid size of 1 mm was attached to the bottom of the slide glass of the PAAM gel, to easily identify indentation points in the center region of the gel (Fig. 3). Then, the gel on the slide glass was placed on the AFM stage, and 400 μL of PBS was dropped on the gel. After placing the AFM probe in PBS on the gel, we waited for one hour before performing the AFM indentation test to minimize thermal drift. The optical level sensitivity and spring constant of the AFM probe were calibrated on the hard surface of the slide glass in PBS. The surface of the gel was indented with respect to the attached grip points, and 10 force-distance curves were obtained per grid point.

Fig. 3 Example of the fabricated PAAM gel with a stiffness gradient, fixed on a slide glass. The grid ruler was attached beneath the cover glass, for AFM indentation mapping

In order to determine E values from the force-distance curves, their approach portion was fitted against the Sneddon model of spherical indenters by using AtomicJ open source software [55]. The Sneddon model of spherical indenters is

$$F = \frac{E}{2(1-v^2)}\left[(a^2 + r^2)\ln\left(\frac{r+a}{r-a}\right) - 2ar\right], \tag{1}$$

$$\delta = \frac{1}{2}a\ln\left(\frac{r+a}{r-a}\right), \tag{2}$$

where F is the indentation force, r is the nominal radius of the AFM probe tip, a is the contact radius between the AFM probe tip and the gel, v is the Poisson's ratio of the PAAM gel (= 0.5), and δ is the indentation depth.

A rheometer (AR 1500ex; TA Instruments, New Castle, DE) was employed to measure the E of the stiff gel [51, 52]. The gel was cast between a 25 mm-diameter stainless steel disk and the rheometer base plate, and its shear modulus (G) was measured by strain amplitude sweep (1 rad/s, 0.1–10% strain) at room temperature. Then, G was converted to E by $E = 2G(1+v)$.

Results

Flow Visualization of Drop Coalescence and Mixing

The proposed fabrication method for hydrogel substrates with stiffness variation relies on limited mixing between two pre-polymer drops in a nearly two-dimensional confinement with a small gap, i.e., the Hele-Shaw cell. In order to confirm the limited mixing in our Hele-Shaw cell, we visualized the coalescence of two water drops and subsequent mixing using color dyes. As shown in Fig. 4(a), one blue drop was placed in one circular hydrophilic well of the bottom plate while one yellow drop was placed in the other well. The front-view image of the two drops shows that the glass surface was hydrophilic. The contact angle of deionized water on the cover glass was measured to be $43 \pm 3°$ (6 μL of diH2O on a cover glass; $N = 10$ measurements) using a goniometer (Model 250; Ramé-hart instrument, NJ). As the top surface was lowered, the drops made a contact with the top glass in a disc shape (Fig. 4(b)). Then, the drops spread out while being squeezed by the lowering top surface.

The expanding speed of the water drop is related with the lowering speed of the top surface as follows. With radius R, the volume of the drop is $V = \pi R^2 h$, where h is the gap distance of the Hele-Shaw cell. Since the drop volume is conserved ($dV/dt = 0$), it is obtained that $2h(dR/dt) = -R(dh/dt)$. Here, $-dh/dt$ is the moving speed of the top surface (= 44.5 μm/s). Then, the Reynolds number of the spreading water disc is $Re = \rho h(dR/dt)/\mu = -\rho R(dh/dt)/2\mu$, where ρ and μ are the density and dynamic viscosity of water, respectively ($\mu/\rho = 1.01 \times 10^{-6}$ m^2/s). Since the radius of the circular well was 5 mm, the maximum Re of

the expanding water drop in the Hele-Shaw cell was 0.11. Therefore, the motion of the expanding water discs was viscosity dominated, and it was slow enough to assume negligible inertia effect prior to coalescence.

When the water drops filled in the circular wells, they expanded and flowed through the straight channel of the hydrophilic region (6 mm wide and 8 mm long; Fig. 2(c)), limited by the superhydrophobic barrier. Eventually, the water drops met near the center of the channel (Fig. 4(c)). On contact, surface-tension-driven coalescence occurred between the water drops, which was set to be $t = 0$ min (Fig. 4(d)). As the coalescence advanced, the merged water drops filled the hydrophilic channel while maintaining the straight interface with distinct color difference. Then, mixing between the two colors took place at the interface, which increased the width of the mixed color zone over time (Fig. 4(e)). This color gradient zone corresponded to the stiffness gradient zone in a fabricated PAAM gel while the blue and yellow colors meant the soft and stiff gels, respectively.

Mixing in the Hele-Shaw Cell

As shown in Fig. 4(e), the color change occurred at the interface between two drops mostly in the x-direction. In contrast, color mixing in the y-direction was insignificant except near the boundary where evaporation- and surface-tension-driven flow could occur. Here, the x- and y-directions are the major and minor axes of the PAAM gel, respectively (Fig. 3). In order to quantify the mixing at the interface, the color value changes at the center were evaluated. The RGB images of Fig. 4(e) were converted to the CMYK mode, and the C (cyan) and Y (yellow) values near the center were averaged in the y direction. Then, the averaged color value of each color was normalized by the average value of the color found in the circular wells. For instance, the average C value was found for the blue drop side well and the yellow drop side well, which are I_{high} and I_{low}, respectively. Then, these two values were used to normalize the y-direction averaged C value near the center; $I^*(x, t) = [I(x, t) - I_{low}]/[I_{high} - I_{low}]$. As shown in Fig. 4(f), I^* for cyan decreased from 1 to 0 in the x direction at the interface while I^* for yellow increased from 0 to 1. Therefore, the color change occurred only at the interface between the two drops, and thus mixing between the two drops was limited.

Figure 4(f) also shows that the mixing zone of each color increased over time, which was expected to be due to diffusion between the two colors. The width of the mixing zone was evaluated by fitting the following one-dimensional (1D) diffusion equation against the measured I^* values [56]:

$$I^*(x, t) = \frac{I(x, t) - I_{low}}{I_{high} - I_{low}} = \frac{1}{2}\text{erfc}\left(\frac{x - x_c}{2\sqrt{Dt}}\right), \tag{3}$$

where x_c is the center of the mixing zone, and D is the diffusion coefficient of one color in the other color. As Fig. 4(f) shows,
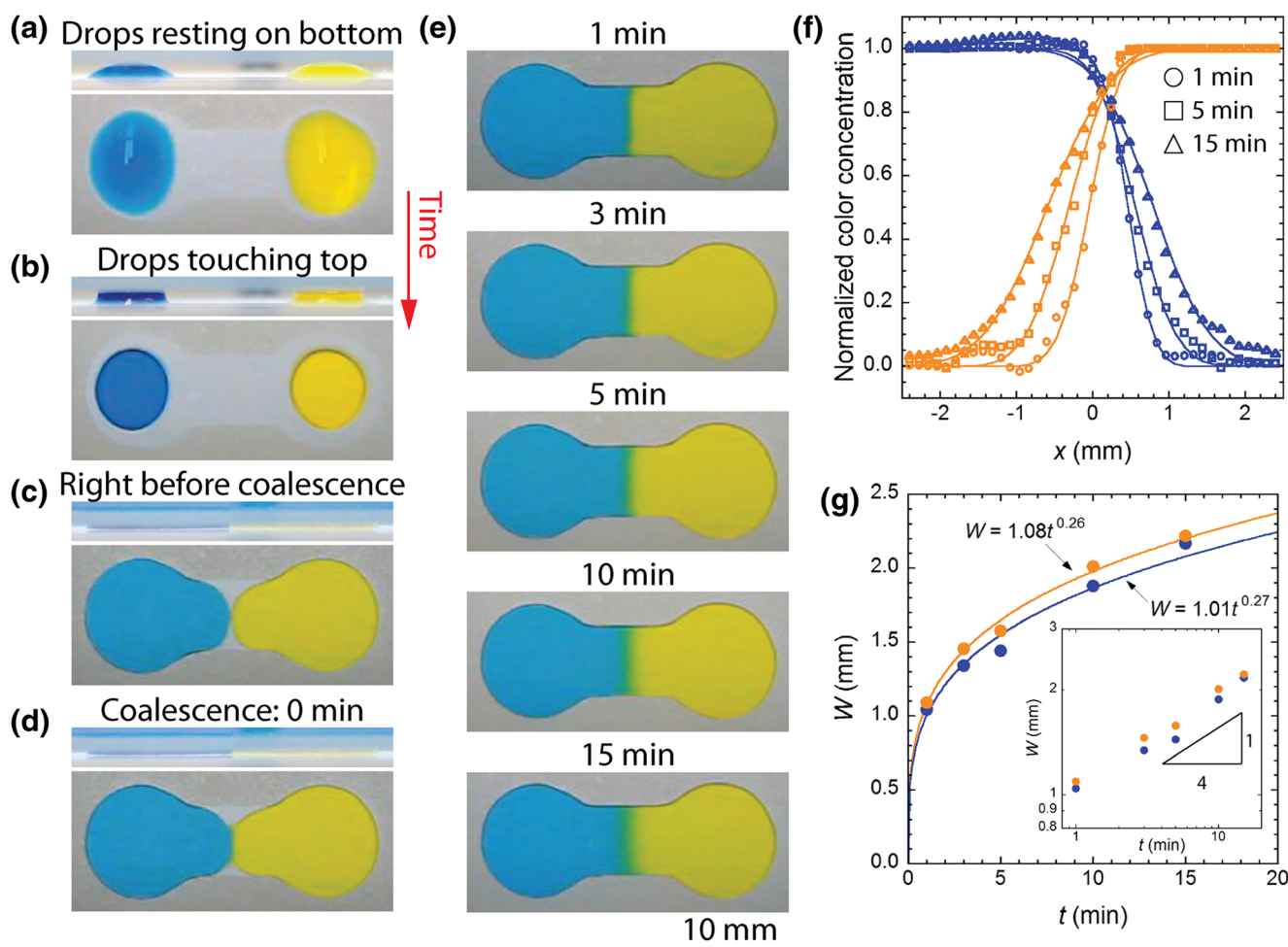
Fig. 4 Water drop coalescence and limited mixing in the Hele-Shaw cell. (A) Colored water drop placed in the circular well areas of the hydrophilic glass region. (B) Water drops touching the top glass surface. (C) Squeezed water drops flowed toward the center, limited by the superhydrophobic barrier, and they were about to coalesce. (D) Water drops coalescing at the center ($t = 0$ min). (E) Progression of mixing between the two colors at the interface. (F) Change of colors (cyan and yellow) in the mixing zone. (G) Width increase of the mixing zone over time. Inset: Log-log scale plot. For (A-D), top image: front view, and bottom image: top view

equation (3) describes the measured color value changes well. The width of the color mixing zone of 90% I^* change was estimated to be $W = |x_{I^*=0.95} - x_{I^*=0.05}|$. Figure 4(g) shows that the width of the color mixing zone was close between cyan and yellow, and it increased with time. Curve fitting using a power function suggests that the temporal increase of the mixing zone width followed $W \sim t^{0.25}$, which is also supported by the log-log plot included in Fig. 4(g). If the color mixing were mainly governed by Fickian diffusion, the width would show $W \sim t^{0.5}$. Therefore, subdiffusion appeared to occur for the mixing in the Hele-Shaw cell.

Stiffness Distribution of PAAM Gels

PAAM gels were successfully fabricated using the proposed method in the Hele-Shaw cell. The fabricated hydrogels had the same dumbbell shape as the superhydrophobic barrier (Fig. 2(c)), which shows that the superhydrophobic barrier

could successfully control and confine the pre-polymer solutions. Regarding the photo-crosslinking of the PAAM gel with UV light, finding the proper intensity of UV light was important because too strong UV light generated cracks on the surface of fabricated PAAM gels.

The stiffness distribution of the fabricated PAAM gels was measured by AFM indentation [52]. The indentation mapping grid was attached to the gel sample's bottom (Fig. 3), and the spherical tip of the colloidal AFM probe indented the gel's top surface according to the grid. The local Young's modulus (E) was determined by applying the Sneddon model [equations (1–2)] to the approach portion of the obtained force-distance curves. As Fig. 5(a) shows, the Sneddon model agreed well with the measured force-indentation depth curves. The measured Young's moduli using the Sneddon model were 2.0–2.3 kPa and 34.0–35.3 kPa for the soft and stiff side of one of the fabricated gels, respectively. These values are close to the nominal E values shown in Table 1: 2.6 kPa and 40.4 kPa.
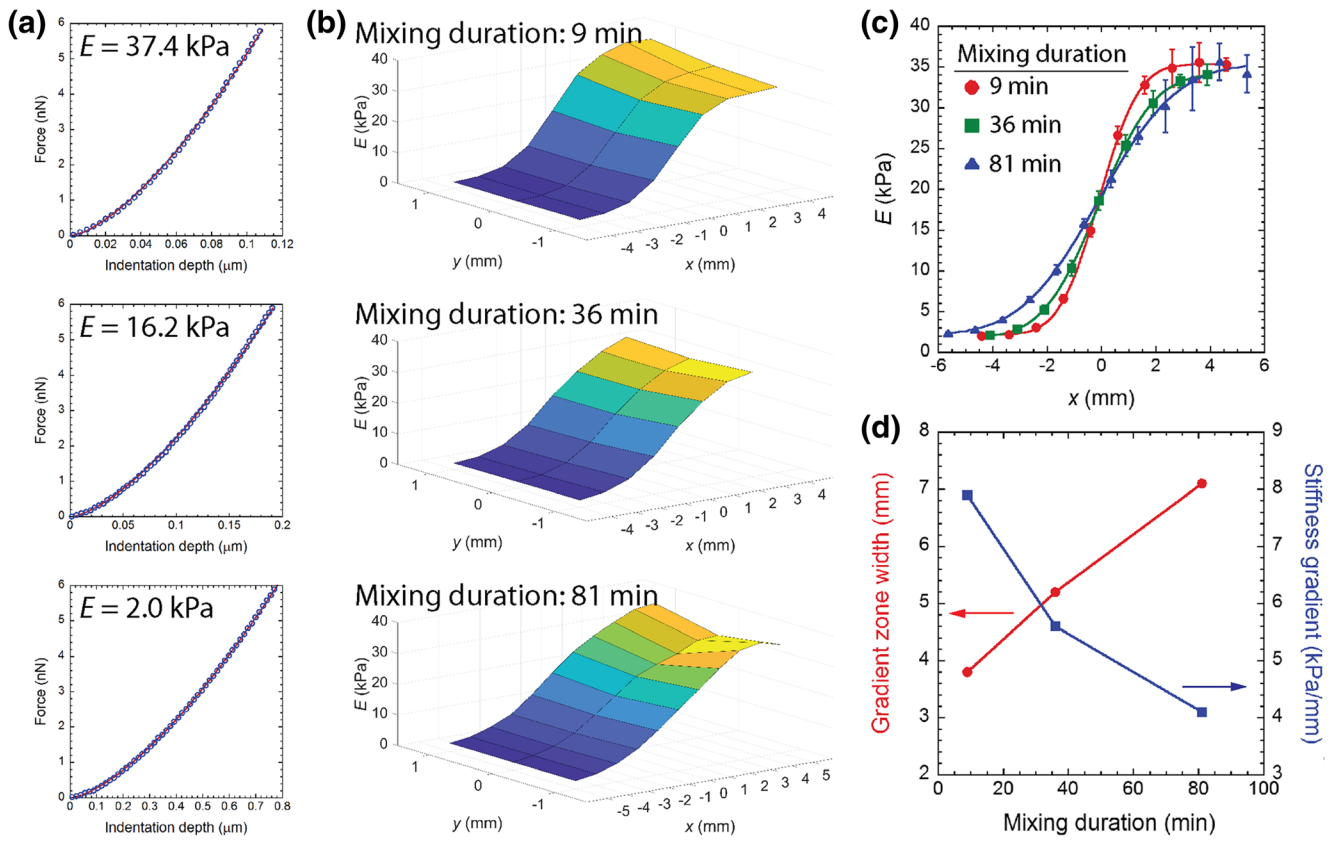
Fig. 5 Stiffness distribution of fabricated PAAM gels. (A) Representative force-indentation depth curves for AFM indentation. (B) Young's modulus distribution of PAAM gels fabricated with different durations of mixing. (C) Average Young's modulus distribution of the PAAM gel samples. Error bar: standard deviation between different *y* locations on one sample. (D) Resultant width of the stiffness gradient zone and the gradient of stiffness

The indentation grid (Fig. 3) enabled indenting the same spots on different gel samples and thus comparing the measure *E* distribution among the gel samples. As shown in Fig. 5(b), the Young's modulus of the gel samples increased from the soft end to the stiff end, and the gel samples had similar *E* values for the ends. Thus, the fabricated gel samples distinctly showed the stiffness gradient zone at the center, and this zone increased in its width as the mixing duration increased. Compared to the drastic change of *E* in the *x*-direction, the *E* value variation in the *y*-direction was negligible. However, this variation became more conspicuous on the stiff side. The *E* variation in the *y*-direction could be due to the flow caused by evaporation and following surface tension change along the boundary, similar to color change in the *y*-direction observed in Fig. 4(e).

In order to determine the stiffness gradient, the measured *E* values were averaged along the *y*-direction as shown in Fig. 5(c). Clearly, the local *E* of the fabricated PAAM gels increased along the *x*-axis of the gel from the soft side to the stiff side, and the deviation in *E* in the *y*-direction increased as the stiffness increased. The gel sample with 9 min-long mixing duration showed evident distinction between the static stiffness zones (two ends of the gel) and the gradient zone (middle of the gel), as expected based on the flow visualization result. As the mixing

duration increased, the gradient zone increased in the width. Concurrently, the two static stiffness zones decreased as shown by the gel samples with longer mixing duration.

Similar to the flow visualization analysis, the following 1D-diffusion-like fitting equation was used to represent the measured *E* distribution:

$$E^*(x) = \frac{E(x) - E_{low}}{E_{high} - E_{low}} = \frac{1}{2}\,\mathrm{erfc}\left(\frac{x - x_c}{2\sqrt{D_{mixing}t_{mixing}}}\right), \quad (4)$$

where E_{high} and E_{low} are the Young's modulus of the stiff and soft regions, respectively, and t_{mixing} is the mixing duration allowed between the coalescence moment and the UV exposure initiation. D_{mixing} can be regarded as the effective diffusion coefficient between the two pre-polymer solution drops. This equation was fitted against the averaged *E* distribution, and it was found that equation (4) could successfully represent the *E* distribution as shown in Fig. 5(c).

One benefit of using equation (4) is that it is possible to identify the center of the stiffness gradient zone (x_c) and to estimate the size of the stiffness gradient zone. As shown in Fig. 5(c), it was found that the gradient zone center of the fabricated gel samples agreed well each other, which indicates that the proposed method maintains quality control and

repeatability in regard to the location of the gradient zone. Similar to the color mixing zone, the size of the stiffness gradient zone is defined to be the x-direction distance for 90% change in E^*: $W = |x_{E^*=0.95} - x_{E^*=0.05}|$. Figure 5(d) shows that W increased with t_{mixing} from 3.8 mm with 9 min-long mixing to 7.1 mm with 81 min-long mixing. Accordingly, the stiffness gradient value ($= [E_{high} - E_{low}]/W$) decreased from 7.9 kPa/mm with 9 min-long mixing to 4.1 kPa/mm with 81 min-long mixing. The obtained stiffness gradient values belong to the typical stiffness gradient range for durotaxis (1–100 kPa/mm) [13, 16, 26, 32, 49]. The y-direction variation of E resulted in the stiffness gradient in the y-direction (0.04–7.72 kPa/mm), and significant E gradient in the y-direction was found mostly in the stiff gel region while the y-direction gradient in the soft gel region and the gradient zone was lower than or close to 1 kPa/mm. The observed range of the y-direction E gradient corresponds to percent changes of 0.3–23.0% over 1 mm distance with respect to local average E values at each x locations. Considering that the straight part of the fabricated gels was about 8 mm long (Fig. 2(c) and 3), the proposed method enabled generating a stiffness gradient across the straight part while keeping the both static stiffness ends of the gel separated.

Discussion

For *in vitro* mechanobiology experiments to mimic the mechanically inhomogeneous *in vivo* environment of the ECM, hydrogels substrates with a spatial variation of stiffness or Young's modulus have been used [11], and various fabrication methods were proposed as briefly summarized in the Introduction. One common principle of the methods is to create a concentration gradient of a hydrogel pre-polymer solution and then to convert the chemical gradient into stiffness gradient via photo-polymerization-based gelation. In this category, the methods using microfluidic concentration gradient generators are most well known [12–17].

The presented study employed limited mixing between two pre-polymer solution drops in the Hele-Shaw cell, i.e., nearly two-dimensional confinement of which the gap height is much smaller than the diameter of the drops, for fabrication of PAAM hydrogels with a stiffness gradient. To the best of our knowledge, Lo et al. first used limited mixing in a narrow confinement formed by two cover glass pieces for this purpose [18]. They placed two PAAM pre-polymer drops of different compositions on a cover glass and placed another cover glass on top of the drops to sandwich and coalesce them. This simple method appears very economical because it could fabricate PAAM gels that had a stiffness gradient between soft and stiff gels and it required neither special equipment nor complicated fabrication steps.

In order to enable modulation of the magnitude of stiffness gradient, we have improved the method of Lo et al. as follows. First, the superhydrophobic barrier was introduced to the bottom glass surface of the Hele-Shaw cell (Fig. 2(c)), to control the location of pre-polymer drops and to guide their motion while being squeezed (Fig. 4(a-e)). The superhydrophobic barrier worked successfully because the drops met near the center of the hydrophilic glass region and the fabricated PAAM gels had the same dumbbell shape as the hydrophilic region (Fig. 3). Second, the squeeze of the drops was controlled by the motorized stage of the Hele-Shaw cell device (Fig. 2(a)). The DC motor and threaded rod of the device enabled lowering the leveled top surface of the Hele-Shaw cell at an average speed of 45 μm/s and slow expansion and flow of the drops in the cell. Therefore, drop coalescence was mainly driven by surface tension without any flow inertia effects, which is important for controlling drop coalescence in the Hele-Shaw cell. Third, the degree of mixing between the two pre-polymer drops was modulated by controlling mixing duration between the drop coalescence and photo-polymerization. Therefore, it was possible to modulate the resultant stiffness gradient of fabricated PAAM gels (Fig. 5(b-d)). Last, the proposed method can be easily adopted because theoretically it requires only a way to control the gap distance between two parallel planes. The Hele-Shaw cell device was built using affordable parts that are commercially available and easily found. For instance, Makeblock parts are available in various sizes and designs, and they are easy to assemble, and an aquarium vacuum pump was used instead of a typical research-purpose vacuum pump.

Because of the small gap height of the Hele-Shaw cell, the mixing in the cell was expected to be governed by diffusion. However, our analyses of the color mixing between water drops show that the width of the color mixing zone grew following $W \sim t^{1/4}$, not $W \sim t^{1/2}$. Also, the diffusion coefficient (D) values of the colors decreased with time while the values were similar between the two colors. The observed subdiffusive spreading of colors could be due to concentration-dependent diffusion in which D decreases with the concentration of the diffusing quantify [57, 58]. In our case, color concentration was represented by color intensity, which decreased with time in the mixing zone. Concentration-dependent diffusion can happen in microchannels, similar to the Hele-Shaw cells, because concentration gradients can be higher than those in macroscale due to the small channel size [59, 60]. The observed non-Fickian diffusion indicates that equation (3) needs to be used with caution although the 1D Fickian diffusion model has been used to describe concentration distribution formed in Hele-Shaw cells [61–64]. In this sense, furthermore, it needs to be pointed out that a conversion of equation (3) to equation (4) was an *ad hoc* approach to determine the width of the stiffness gradient zone. As Fig. 5(d) shows, the stiffness gradient zone of the PAAM gels increased almost linearly with mixing time, not following a

power law. This is presumably due to continued diffusion during long photo-polymerization.

It was noted that the measured E values of the stiff gel (34.0–35.3 kPa) were a little lower than the known nominal E value (40.4 kPa). This difference could be due to the fact that the resultant E of PAAM gel is affected by gel fabrication steps and environmental factors such as humidity and temperature [65, 66]. Accordingly, we measured the E of the stiff gel using the rheometer [51, 52], and the measured E value was 36.8 ± 0.3 kPa ($N = 5$ measurements), close to our AFM measurement.

It also needs to be noted that measured E values depend on the value of gel Poisson's ratio (ν). We used $\nu = 0.5$ because this value has been frequently used for PAAM gels [32, 33, 65, 67–70], but other values were also used, such as $\nu = 0.3$ in [18, 71] and $\nu = 0.46$ in [72]. It is known that the ν of PAAM gel can differ depending on the time- and length- scale of measurements because of solvent escape from gel [73, 74], and the short-time gel Poisson's ratio is known to be 0.5 [75]. The contact time between the AFM probe tip and the gel was estimated by dividing the sum of the indention depth and the probe deflection with the probe speed, and it was about 0.9 s for the soft gel and about 0.2 s for the stiff gel. Considering that the relaxation of PAAM gel takes a few seconds in microscale indentation [74], the AFM probe tip made short-time contacts with the gel during indentation, and thus $\nu = 0.5$ appears to be an appropriate choice for Poisson's ratio.

Conclusion

There are various methods to fabricate hydrogel substrates with stiffness variation or gradients for cell mechanobiology studies. In this study, we have improved the mixing-based method of Lo et al. [18] in which two pre-polymer drops of different stiffness values were squeezed between two glass surfaces, by better controlling liquid drop squeeze, coalescence and diffusion-based mixing using the superhydrophobic barrier and the lab-built Hele-Shaw cell device. Flow visualization using colored water drops shows limited mixing between the drops after coalescence and suggests the mixing is driven by diffusion. The Young's modulus distribution of fabricated PAAM gel samples was measured using AFM indentation, and it shows that the two ends of the gel samples retain low and high E values while their center part has a clear zone of increasing stiffness.

References

1. Discher DE, Janmey P, Wang Y-L (2005) Tissue cells feel and respond to the stiffness of their substrate. Science 310:1139–1143
2. Watt FM, Huck WTS (2013) Role of the extracellular matrix in regulating stem cell fate. Nat Rev Mol Cell Biol 14:467–473
3. Charras G, Sahai E (2014) Physical influences of the extracellular environment on cell migration. Nat Rev Mol Cell Biol 15:813–824
4. Janson IA, Putnam AJ (2014) Extracellular matrix elasticity and topography: material-based cues that affect cell function via conserved mechanisms. J Biomed Mater Res A 103:1248–1258
5. Levental I, Georges PC, Janmey PA (2007) Soft biological materials and their impact on cell function. Soft Matt 3:299–306
6. Trappmann B, Chen CS (2013) How cells sense extracellular matrix stiffness: a material's perspective. Curr Op Biotechnol 24:948–953
7. Wen JH, Vincent LG, Fuhrmann A, Choi YS, Hribar KC, Taylor-Weiner H, Chen S, Engler AJ (2014) Interplay of matrix stiffness and protein tethering in stem cell differentiation. Nat Mater 13:979–987
8. Engler AJ, Sen S, Sweeney HL, Discher DE (2006) Matrix elasticity directs stem cell lineage specification. Cell 126:677–689
9. Yeung T, Georges PC, Flanagan LA, Marg B, Ortiz M, Funaki M, Zahir N, Ming W, Weaver V, Janmey PA (2005) Effects of substrate stiffness on cell morphology, cytoskeletal structure, and adhesion. Cell Motil Cytoskel 60:24–34
10. Chen L, Zhang Z, Qiu J, Zhang L, Luo X, Jang J (2014) Chaperonin CCT-mediated AIB1 folding promotes the growth of ERα-positive breast cancer cells on hard substrates. PLoS One 9:e96085
11. Whang M, Kim J (2016) Synthetic hydrogels with stiffness gradients for durotaxis study and tissue engineering scaffolds. Tissue Eng Regen Med 13:126–139
12. Burdick JA, Khademhosseini A, Langer R (2004) Fabrication of gradient hydrogels using a microfluidics/photopolymerization process. Langmuir 20:5153–5156
13. Zaari N, Rajagopalan P, Kim SK, Engler AJ, Wong JY (2004) Photopolymerization in microfluidic gradient generators: microscale control of substrate compliance to manipulate cell response. Adv Mater 16:2133–2137
14. Sundararaghavan HG, Monteiro GA, Firestein BL, Shreiber DI (2009) Neurite growth in 3D collagen gels with gradients of mechanical properties. Biotechnol Bioeng 102:632–643
15. Byfield FJ, Wen Q, Levental I, Nordstrom K, Arratia PE, Miller RT, Janmey PA (2009) Absence of filamin a prevents cells from responding to stiffness gradients on gels coated with collagen but not fibronectin. Biophys J 96:5095–5102
16. Isenberg BC, DiMilla PA, Walker M, Kim S, Wong JY (2009) Vascular smooth muscle cell durotaxis depends on substrate stiffness graident strength. Biophys J 97:1313–1322
17. Orsi G, Fagnano M, De Maria C, Montemurro F, Vozzi G (2017) A new 3D concentration gradient maker and its application in building hydrogels with a 3D stiffness gradient. J Tissue Eng Regen Med 11:256–264
18. Lo C-M, Wang H-B, Dembo M, Wang Y-L (2000) Cell movement is guided by the rigidity of the substrate. Biophys J 79:144–152
19. Wang H-B, Dembo M, Hanks SK, Wang Y-I (2001) Focal adhesion kinase is involved in mechanosensing during fibroblast migration. Proc Natl Acad Sci U S A 98:11295–11300
20. Raab M, Swift J, Dingal PCDP, Shah P, Shin J-W, Discher DE (2012) Crawling from soft to stiff matrix polarizes the cytoskeleton

and phosphoregulates myosin-II heavy chain. J Cell Biol 199:669–683

21. Nemir S, Hayenga HN, West JL (2010) PEGDA hydrogels with patterned elasticity: novel tools for the study of cell response to substrate rigidity. Biotechnol Bioeng 105:636–644

22. Diederich VEG, Studer P, Kern A, Lattuada M, Storti G, Sharma RI, Snedeker JG, Morbidelli M (2013) Bioactive polyacrylamide hydrogels with gradients in mechanical stiffness. Biotechnol Bioeng 110:1508–1519

23. Du Y, Hancock MJ, He J, Villa-Uribe JL, Wang B, Cropek DM, Khademhosseini A (2010) Convection-driven generation of long-range material gradients. Biomaterials 31:2686–2694

24. Wong JY, Velasco A, Rajagopalan P, Pham Q (2003) Directed movement of vascular smooth muscle cells on gradient-compliant hydrogels. Langmuir 19:1908–1913

25. Kidoaki S, Matsuda T (2008) Microelastic gradient gelatinous gels to induce cellular mechanotaxis. J Biotechnol 133:225–230

26. Tse JR, Engler AJ (2011) Stiffness gradients mimicking *in vivo* tissue variation regulate mesenchymal stem cell fate. PLoS One 6: e15978

27. Marklein RA, Burdick JA (2010) Spatially controlled hydrogel mechanics to modulate stem cell interactions. Soft Matt 6:136–143

28. Khetan S, Burdick JA (2010) Patterning network structure to spatially control cellular remodeling and stem cell fate within 3-dimensional hydrogels. Biomaterials 31:8228–8234

29. Stowers RS, Allen SC, Suggs LJ (2015) Dynamic phototuning of 3D hydrogel stiffness. Proc Natl Acad Sci U S A 112:1953–1958

30. Kloxin AM, Benton JA, Anseth KS (2010) *In situ* elasticity modulation with dynamic substrates to direct cell phenotype. Biomaterials 31:1–8

31. Johnson PM, Reynolds TB, Stansbury JW, Bowman CN (2005) High throughput kinetic analysis of photopolymer conversion using composition and exposure time gradients. Polymer 46:3300–3306

32. Sunyer R, Jin AJ, Nossal R, Sackett DL (2012) Fabrication of hydrogels with steep stiffness gradients for studying cell mechanical response. PLoS One 7:e46107

33. García S, Sunyer R, Olivares A, Noailly J, Atencia J, Trepat X (2015) Generation of stable orthogonal graidents of chemical concentration and substrate stiffness in a microfluidic device. Lab Chip 15:2606–2614

34. Kloxin AM, Tibbitt MW, Kasko AM, Fairbairn JA, Anseth KS (2010) Tunable hydrogels for external manipulation of cellular microenvironments through controlled photodegradation. Adv Mater 22:61–66

35. Tong X, Jiang J, Zhu D, Yang F (2016) Hydrogels with dual gradients of mechanical and biochemical cues for deciphering cell-niche interactions. ACS Biomater Sci Eng 2:845–852

36. Yanagawa F, Mizutani T, Sugiura S, Takagi T, Sumaru K, Kanamori T (2015) Partially photodegradable hybrid hydrogels with elasticity tunable by light irradiation. Colloid Surf B 126:575–579

37. Kawano T, Kidoaki S (2011) Elasticity boundary conditions required for cell mechanotaxis on microelastically-patterned gels. Biomaterials 32:2725–2733

38. Mosiewicz KA, Kolb L, van der Vlies AJ, Lutolf MP (2014) Microscale patterning of hydrogel stiffness through light-triggered uncaging of thiols. Biomater Sci 2:1640–1651

39. Frey MT, Wang Y-L (2009) A photo-modulatable material for probing cellular responses to substrate rigidity. Soft Matt 5:1918–1924

40. Wang P-Y, Tsai W-B, Voelcker NH (2012) Screening of rat mesenchymal stem cell behaviour on polydimethylsiloxane stiffness gradients. Acta Biomater 8:519–530

41. Gray DS, Tien J, Chen CS (2003) Repositioning of cells by mechanotaxis on surfaces with micropatterned Young's modulus. J Biomed Mater Res A 66:605–614

42. Choi YS, Vincent LG, Lee AR, Kretchmer KC, Chirasatitsin S, Dobke MK, Engler AJ (2012) The alignment and fusion assembly of adipose-derived stem cells on mechanically patterned matrices. Biomaterials 33:6943–6951

43. Cheung YK, Azeloglu EU, Shiovitz DA, Costa KD, Seliktar D, Sia SK (2009) Microscale control of stiffness in a cell-adhesive substrate using microfluidics-based lithography. Angew Chem Int Ed 48:7188–7192

44. Shu Y, Chan HN, Guan D, Wu H, Ma L (2017) A simple fabricated thickness-based stiffness gradient for cell studies. Sci Bull 62:222–228

45. Kuo C-HR, Xian J, Brenton JD, Franze K, Sivaniah E (2012) Complex stiffness gradient substrates for studying mechanotatic cell migration. Adv Mater 24:6059–6064

46. Chao PG, Sheng S-C, Chang W-R (2014) Micro-composite substrates for the study of cell-matrix mechanical interactions. J Mech Behav Biomed Mater 38:232–241

47. Kim TH, An DB, Oh SH, Kang MK, Song HH, Lee JH (2015) Creating stiffness gradient polyvinyl alcohol hydrogel using a simple gradual freezing-thawing method to investigate stem cell differentiation behaviors. Biomaterials 40:51–60

48. Hopp I, Michelmore A, Smith LE, Robinson DE, Bachhuka A, Mierczynska A, Vasilev K (2013) The influence of substrate stiffness gradients on primary human dermal fibroblasts. Biomaterials 34:5070–5077

49. Tse JR, Engler AJ (2010) Preparation of hydrogel substrates with tunable mechanical properties. In: Current protocols in cell biology. John Wiley & Sons, Inc: 1–16

50. Lakins JN, Chin AR, Weaver VM (2012) Exploring the link between human embryonic stem cell organization and fate using tension-calibrated extracellular matrix functionalized polyacrylamide gels. In: Mace KA, Braun KM (eds) Progenitor cells, vol 916. Methods in molecular biology. Humana Press, Totawa, pp 317–350

51. Lee D, Rahman MM, Zhou Y, Ryu S (2015) Three-dimensional confocal microscopy indentation method for hydrogel elasticity measurement. Langmuir 31:9684–9693

52. Lee D, Ryu S (2017) A validation study of the repeatability and accuracy of atomic force microscopy indentation using polyacrylamide gels and colloidal probes. J Biomech Eng 139:044502

53. Graham PJ, Farhangi MM, Dolatabadi A (2012) Dynamics of droplet coalescence in response to increasing hydrophobicity. Phys Fluids 24:112105

54. Hancock MJ, Yanagawa F, Jang Y-H, He J, Kachouie NN, Kaji H, Khademhosseini A (2012) Designer hydrophilic regions regulate droplet shape for controlled surface patterning and 3D microgel synthesis. Small 8:393–403

55. Hermanowicz P, Sarna M, Burda K, Gabryś H (2014) AtomicJ: an open source software for analysis of force curves. Rev Sci Instrum 85:063703

56. Crank J (1975) The mathematics of diffusion. 2nd edn. Oxford University Press, Oxford, UK

57. Carey AE, Wheatcraft SW, Glass RJ, O'Rourke JP (1995) Non-Fickian ionic diffusion across high-concentration gradient. Water Resour Res 31:2213–2218

58. Küntz M, Lavallée P (2004) Anomalous diffusion is the rule in concentration-dependent diffusion processes. J Phys D Appl Phys 37:L5–L8

59. Wu Z, Nguyen N-T, Huang X (2004) Nonlinear diffusive mixing in microchannels: theory and experiments. J Micromech Microeng 14: 604–611

60. Chen J, Kim HD, Kim KC (2013) Measurement of dissolved oxygen diffusion coefficient in a microchannel using UV-LED induced fluorescent method. Microfluid Nanofluid 14:541–550

61. Jimenez M, Dietrich N, Cockx A, Hébrard G (2013) Experimental study of O_2 diffusion coefficient measurement at a planar gas-liquid interface by planar laser-induced fluorescence with inhibition. AICHE J 59:325–333

62. Jimenez M, Dietrich N, Grace JR, Hébrard G (2014) Oxgen mass transfer and hydrodynamic behaviour in wastewater: determination of local impact of surfactants by visualization techniques. Water Res 58:111–121

63. Roht YL, Auradou H, Hulin J-P, Salin D, Chertcoff R, Ippolito I (2015) Time dependence and local structure of tracer dispersion in oscillating liquid hele-Shaw flows. Phys Fluids 27:103602

64. Xu F, Jimenez M, Dietrich N, Hébrard G (2017) Fast determination of gas-liquid diffusion coefficient by an innovative double approach. Chem Eng Sci 170:68–76

65. Long R, Hall MS, Wu M, Hui C-Y (2011) Effects of gel thickness on microscopic indentation measurements of gel modulus. Biophys J 101:643–650

66. Calvet D, Wong JY, Giasson S (2004) Rheological monitoring of polyacrylamide gelation: importance of cross-link density and temperature. Macromolecules 37:7762–7771

67. Buxboim A, Rajagopalan K, Brown AEX, Discher DE (2010) How deeply cells feel: methods for thin gels. J Phys Condens Matter 22:194116

68. Markert CD, Guo X, Skardal A, Wang Z, haradwaj S, Zhang Y, Bonin K, Guthold M (2013) Characterizaing the micro-scale elastic modulus of hydrogels for use in regenerative medicine. J Mech Behav Biomed Mater 27:115–127

69. Abidine Y, Laurent VM, Michel R, Duperray A, Palade LI, Verdier C (2015) Physical properties of polyacrylamide gels probed by AFM and rheology. Eur Phys Lett 109:38003

70. Boudou T, Ohayon J, Picart C, Tracqui P (2006) An extended relationship for the characterization of Young's modulus and Poisson's ratio of tunable polyacrylamide gels. Biorheology 43:721–728

71. Damljanovic V, Lagerholm BC, Jacobson K (2005) Bulk and micropatterned conjugation of extracellular matrix proteins to characterized polyacrylamide substrates for cell mechanotransduction assays. Biotechniques 39:847–851

72. Takigawa T, Morino Y, Urayama K, Masuda T (1996) Poisson's ratio of polyacrylamide (PAAm) gels. Polym Gel Netw 4:1–5

73. Geissler E, Hecht AM (1980) The Poisson ratio in polymer gels. Macromolecules 13:1276–1280

74. Kalcioglu ZI, Mahmoodian R, Hu Y, Suo Z, Van Vliet KJ (2012) From macro- to microscale poroelastic characterization of polymeric hydrogels *via* indentation. Soft Matt 8:3393–3398

75. Geissler E, Hecht AM (1981) The Poisson ratio in polymer gels. 2. Macromolecules 14:185–188